Available online at www.sciencedirect.com
ScienceDirect
Comput. Methods Appl. Mech. Engrg. 309 (2016) 680–692
Computer methods in applied mechanics and engineering
www.elsevier.com/locate/cma

Elimination of self-straining in isogeometric formulations of curved Timoshenko beams in curvilinear coordinates

Myung-Jin Choi, Seonho Cho*

Department of Naval Architecture and Ocean Engineering, Seoul National University, 1 Gwanak-ro, Gwanak-gu, Seoul 151-744, Republic of Korea

Received 3 April 2016; received in revised form 15 July 2016; accepted 17 July 2016
Available online 25 July 2016

Highlights

- Isogeometric invariant formulation to eliminate self-straining in curved beams.
- Self-straining deteriorates response quality due to a failure in rigid body motion.
- Discretization of global displacement can resolve the self-straining completely.
- Combination with SRI and B-bar methods to alleviate membrane and shear locking.

Abstract

Isogeometric formulations of curved Timoshenko beams in curvilinear coordinates often result in self-straining of membrane and shear strains, due to the discretization of the local displacement field. Self-straining means a failure in exact representation of rigid body motions, which consequently deteriorates response quality. To overcome the difficulty of self-straining, we propose an invariant formulation that discretizes the global displacement field. It turns out that the approximated membrane, shear, and bending strain measures are invariant regardless of initial geometry in the proposed formulation. For effective applications to any arbitrarily curved structures and locking-free formulations to alleviate membrane and shear locking, the proposed invariant formulation is combined with selective reduced integration (SRI) and $\bar{B}$ projection method. Numerical examples demonstrate the effectiveness and applicability of the proposed invariant formulation, which gives much more accurate results together with both SRI and $\bar{B}$ projection method, in comparison to the existing isogeometric formulations.

Keywords: Curvilinear coordinates; Self-straining; Isogeometric analysis; Curved Timoshenko beam; Selective reduced integration; $\bar{B}$ projection method

1. Introduction

Membrane and shear locking mean the inability to represent the "inextensible bending" and "shearless bending", respectively. Bouclier et al. [1] and Adam et al. [2] suggested locking-free isogeometric formulations of curved Timoshenko beams in curvilinear coordinates. The local displacement field is discretized to obtain the approximated membrane and shear strains. However, these strain measures generally fail to pass the patch test of rigid body motions, which is called as self-straining [3]. Especially as the initial curvature variation of the beam increases, this self-straining triggers severe numerical instabilities that prevent locking-free formulations in [1,2] from being utilized

* Corresponding author. Fax: +82 2 888 9298.
E-mail address: secho@snu.ac.kr (S. Cho).

http://dx.doi.org/10.1016/j.cma.2016.07.019
0045-7825/

for arbitrarily curved beams. Armero and Valverde [3] showed that, in a finite element context for the curved Kirchhoff beam analysis using Hermite basis functions, the classical elements which interpolate the axial and the transversal displacement components separately do not represent the rigid body motions exactly. In this paper, shear deformable beams are considered for the isogeometric analysis using NURBS basis functions. We discuss a discretization scheme together with locking-free formulations to overcome the aforementioned difficulties; self-straining and membrane and shear locking.

This paper is organized as follows: in Section 2.1, we prove the invariance of the strain measures in continuum form. In Section 2.2, we investigate self-straining of the approximated strain measures. In Section 3, a formulation to eliminate self-straining is suggested. In Section 4, through numerical examples, we demonstrate self-straining phenomenon and its elimination employing the proposed formulation.

2. Self-straining in curved Timoshenko beams

2.1. Invariance of strain measures in continuum form

The global displacement vector $\hat{\mathbf{z}}$ is expressed in curvilinear frame as

$$\hat{\mathbf{z}} = z_1\mathbf{j}_1 + z_2\mathbf{j}_2, \tag{1}$$

where $\mathbf{j}_1$ and $\mathbf{j}_2$ are the unit tangential and normal vectors, respectively. The following strain measures can be derived, from the equilibrium equations and the principle of virtual work [3], as

$$\left.\begin{aligned} \varepsilon_m &= z_{1,s} - kz_2 \\ \gamma_s &= kz_1 + z_{2,s} - \theta_b \\ \omega_b &= \theta_{b,s} \end{aligned}\right\}, \tag{2}$$

where ε_m, γ_s, and ω_b are the membrane, shear, and bending strain measures, respectively. $(\bullet)_{,s}$ denotes a differentiation with respect to the arc-length coordinate s. k and θ_b represent the initial curvature and the rotation angle of cross-section, respectively. Combining the Frenet–Serret formulas ($\mathbf{j}_{1,s} = k\mathbf{j}_2$, $\mathbf{j}_{2,s} = -k\mathbf{j}_1$) with the derivative of Eq. (1) with respect to s, Eq. (2) can be rewritten as

$$\left.\begin{aligned} \varepsilon_m &= \hat{\mathbf{z}}_{,s} \cdot \mathbf{j}_1 \\ \gamma_s &= \hat{\mathbf{z}}_{,s} \cdot \mathbf{j}_2 - \theta_b \\ \omega_b &= \theta_{b,s} \end{aligned}\right\}. \tag{3}$$

To prove the invariance of Eq. (3), take a rigid body translation given by an arbitrary constant vector $\hat{\mathbf{z}} = \mathbf{c}_T \in \mathbf{R}^2$ and a rotation angle $\theta_b = c_R = 0$. Then, for all $\mathbf{c}_T \in \mathbf{R}^2$, Eq. (3) satisfies the following:

$$\left.\begin{aligned} \varepsilon_m &= \mathbf{c}_{T,s} \cdot \mathbf{j}_1 = 0 \\ \gamma_s &= \mathbf{c}_{T,s} \cdot \mathbf{j}_2 - c_R = 0 \\ \omega_b &= c_{R,s} = 0 \end{aligned}\right\}. \tag{4}$$

Next, consider an infinitesimal rigid body rotation $\theta_b = c_R$ expressed by the constant rotation angle and the associated displacement vector as

$$\hat{\mathbf{z}} = (\mathbf{X} - \mathbf{X}_{ref}) \times \boldsymbol{\theta} = c_R\tilde{\mathbf{I}}(\mathbf{X} - \mathbf{X}_{ref}), \quad \text{where } \tilde{\mathbf{I}} \equiv \begin{bmatrix} 0 & -1 \\ 1 & 0 \end{bmatrix}. \tag{5}$$

$\boldsymbol{\theta} \equiv [0, 0, c_R]^T$ denotes the infinitesimal rotation vector. $\mathbf{X}, \mathbf{X}_{ref} \in \mathbf{R}^2$ represent the position vectors of a point on the neutral axis and a reference point, respectively. Substituting Eq. (5) into Eq. (3) leads to

$$\left.\begin{aligned} \varepsilon_m &= \theta_b\tilde{\mathbf{I}}\mathbf{X}_{,s} \cdot \mathbf{j}_1 = \theta_b\mathbf{j}_2 \cdot \mathbf{j}_1 = 0 \\ \gamma_s &= \theta_b\tilde{\mathbf{I}}\mathbf{X}_{,s} \cdot \mathbf{j}_2 - \theta_b = 0 \\ \omega_b &= c_{R,s} = 0 \end{aligned}\right\}, \tag{6}$$

for all $c_R \in \mathbf{R}$ and $\mathbf{X}_{ref} \in \mathbf{R}^2$, since $\mathbf{X}_{,s} = \mathbf{j}_1$ due to the arc-length parameterization and the orthonormal vectors $\mathbf{j}_1$ and $\mathbf{j}_2$ are related by $\mathbf{j}_2 = \tilde{\mathbf{I}}\mathbf{j}_1$.

Observation 1. The strain measures in Eqs. (2) and (3) are equivalent to each other and invariant. However, after the approximation using the NURBS basis functions, it depends on the discretization manner whether the approximated strain measures are still invariant or not.

2.2. Non-invariance of strain measures in discrete form

Bouclier et al. [1] and Adam et al. [2] discretized the displacement component vector and the rotation as follows:

$$\mathbf{z}^h = \sum_{I=1}^{n} W_I(\xi)\mathbf{y}_I \tag{7}$$

and

$$\theta_b^h = \sum_{I=1}^{n} W_I(\xi)\theta_{bI}, \tag{8}$$

where W_I and ξ are the Ith NURBS basis function and the parametric coordinate, respectively. $\mathbf{y}_I$ and θ_{bI} are the response coefficients corresponding to the Ith control point. n is the total number of the NURBS basis functions. Using Eqs. (7) and (8), the strain fields in Eq. (2) are approximated as

$$\varepsilon_m^h = \sum_{I=1}^{n}(W_{I,s}y_{1I} - kW_I y_{2I}), \tag{9}$$

$$\gamma_s^h = \sum_{I=1}^{n}(kW_I y_{1I} + W_{I,s}y_{2I} - W_I\theta_{bI}), \tag{10}$$

and

$$\omega_b^h = \sum_{I=1}^{n} W_{I,s}\theta_{bI}, \tag{11}$$

where $W_{I,s} = W_{I,\xi}/J_{cb}$, $J_{cb} \equiv s_{,\xi} = \left\|\mathbf{X}_{,\xi}\right\|$, and $\mathbf{X}$ represents the neutral axis curve. The rotation coefficient θ_{bI} represents the rotation of control net, which is related to the rotation of physical domain by the affine covariance property of NURBS basis function [4]. In contrast, the displacement component coefficient $\mathbf{y}_I = [y_{1I}, y_{2I}]^T$ has no physical significance so that it needs to be expressed by the global displacement vector, which requires constructing the following two linear systems of n equations due to the non-interpolatory characteristic of the NURBS basis function.

$$\left.\begin{aligned} z_1^h(\bar{\xi}_i) &= \sum_{I=1}^{n} W_I(\bar{\xi}_i)y_{1I} = \sum_{I=1}^{n} A_{iI}y_{1I} \\ z_2^h(\bar{\xi}_i) &= \sum_{I=1}^{n} W_I(\bar{\xi}_i)y_{2I} = \sum_{I=1}^{n} A_{iI}y_{2I} \end{aligned}\right\}, \tag{12}$$

where $A_{iI} \equiv W_I(\bar{\xi}_i)$ are the components of collocation matrix and the positions of the collocation points $\bar{\xi}_i$ $(i = 1 \sim n)$ are determined, by the Greville abscissae, as

$$\bar{\xi}_i = \frac{1}{p}(\xi_{i+1} + \xi_{i+2} + \cdots + \xi_{i+p}), \tag{13}$$

where p is the degree of NURBS basis functions. Using Eq. (12) and the relation of Eq. (1), the displacement coefficients can be expressed as

$$\left.\begin{aligned} y_{1I} &= \sum_{i=1}^{n} A_{Ii}^{-1} z_1^h(\bar{\xi}_i) = \sum_{i=1}^{n} A_{Ii}^{-1}\mathbf{j}_1{}^T(\bar{\xi}_i)\hat{\mathbf{z}}^h(\bar{\xi}_i) \\ y_{2I} &= \sum_{i=1}^{n} A_{Ii}^{-1} z_2^h(\bar{\xi}_i) = \sum_{i=1}^{n} A_{Ii}^{-1}\mathbf{j}_2{}^T(\bar{\xi}_i)\hat{\mathbf{z}}^h(\bar{\xi}_i) \end{aligned}\right\}, \tag{14}$$

where A_{Ii}^{-1} are the components of inverse matrix. Substituting Eq. (14) into Eqs. (9) and (10), we have the following:

$$\varepsilon_m^h = \sum_{I=1}^{n}\sum_{i=1}^{n}\left\{W_{I,s}A_{Ii}^{-1}\mathbf{j}_1{}^T(\bar{\xi}_i) - kW_I A_{Ii}^{-1}\mathbf{j}_2{}^T(\bar{\xi}_i)\right\}\hat{\mathbf{z}}^h(\bar{\xi}_i) \tag{15}$$

and

$$\gamma_s^h = \sum_{I=1}^{n}\sum_{i=1}^{n}\left\{kW_I A_{Ii}^{-1}\mathbf{j}_1{}^T(\bar{\xi}_i) + W_{I,s}A_{Ii}^{-1}\mathbf{j}_2{}^T(\bar{\xi}_i)\right\}\hat{\mathbf{z}}^h(\bar{\xi}_i) - \sum_{i=1}^{n} W_I\theta_{bI}. \tag{16}$$

To investigate the non-invariance of the approximated strain measures, consider the rigid body translation as

$$\left.\begin{array}{l}\hat{\mathbf{z}}^h(\bar{\xi}_i) = \mathbf{c}_T \\ \theta_{bI} = \theta_b^h = c_R = 0\end{array}\right\} \quad (i, I = 1 \sim n), \tag{17}$$

where the relation $\theta_{bI} = \theta_b^h$ is obtained from the affine covariance property of the NURBS basis function. Substituting Eq. (17) into Eqs. (15), (16), and (11) yields the following:

$$\varepsilon_m^h = \mathbf{c}_T{}^T\sum_{I=1}^{n}\sum_{i=1}^{n}\left\{W_{I,s}A_{Ii}^{-1}\mathbf{j}_1(\bar{\xi}_i) - kW_I A_{Ii}^{-1}\mathbf{j}_2(\bar{\xi}_i)\right\} \equiv \mathbf{c}_T{}^T\mathbf{a}, \tag{18}$$

$$\gamma_s^h = \mathbf{c}_T{}^T\sum_{I=1}^{n}\sum_{i=1}^{n}\left\{kW_I A_{Ii}^{-1}\mathbf{j}_1(\bar{\xi}_i) + W_{I,s}A_{Ii}^{-1}\mathbf{j}_2(\bar{\xi}_i)\right\} = \mathbf{c}_T{}^T(\tilde{\mathbf{I}}\mathbf{a}), \tag{19}$$

and $\omega_b^h = 0$. The vector function $\mathbf{a} = \mathbf{a}(\xi)$ generally does not vanish. However, if the initial geometry is circular or straight, it can be proved that the vector function vanishes. First, for a circular geometry, the unit tangential and normal vectors are expressed as:

$$\left.\begin{array}{l}\mathbf{j}_2 = (\mathbf{X}_c - \mathbf{X})/R = k(\mathbf{X}_c - \mathbf{X}) \\ \mathbf{j}_1 = -\tilde{\mathbf{I}}\mathbf{j}_2 = -k\tilde{\mathbf{I}}(\mathbf{X}_c - \mathbf{X})\end{array}\right\}, \tag{20}$$

where $\mathbf{X}_c$ and R denote the center position and radius of a circle, respectively, and the relation $k = 1/R$ is used. Substituting Eq. (20) into the expression of the vector $\mathbf{a}$ in Eq. (18), and using the partition of unity of NURBS basis functions, the vector $\mathbf{a}$ is rewritten as

$$\begin{aligned}\mathbf{a} &= -k\sum_{I=1}^{n}\sum_{i=1}^{n}\left[-W_{I,s}A_{Ii}^{-1}\tilde{\mathbf{I}}\mathbf{X}(\bar{\xi}_i) + kW_I A_{Ii}^{-1}\left\{\mathbf{X}_c - \mathbf{X}(\bar{\xi}_i)\right\}\right] - k\tilde{\mathbf{I}}\mathbf{X}_c\sum_{I=1}^{n} W_{I,s} \\ &= -k\sum_{I=1}^{n}\left\{-W_{I,s}\tilde{\mathbf{I}}\mathbf{B}_I + kW_I(\mathbf{X}_c - \mathbf{B}_I)\right\},\end{aligned} \tag{21}$$

where $\mathbf{B}_I$ denotes the position of Ith control point. Then, using the relation $\mathbf{X}_{,s} = \sum_{I=1}^{n} W_{I,s}\mathbf{B}_I = \mathbf{j}_1$ and Eq. (20), we have the following:

$$\mathbf{a} = -k\left\{-\tilde{\mathbf{I}}\mathbf{j}_1 + k(\mathbf{X}_c - \mathbf{X})\right\} = -k(-\tilde{\mathbf{I}}\mathbf{j}_1 + \mathbf{j}_2) = \mathbf{0}. \tag{22}$$

Thus, $\varepsilon_m^h = \gamma_s^h = \omega_b^h = 0$ for any $\mathbf{c}_T \in \mathbf{R}^2$, if the initial geometry is circular. Second, if the initial geometry is straight ($k = 0$), $\mathbf{j}_1$ is a constant vector so that we have the following:

$$\mathbf{a} = \sum_{I=1}^{n} W_{I,s}\left(\sum_{i=1}^{n} A_{Ii}^{-1}\mathbf{j}_1\right) = \sum_{I=1}^{n} W_{I,s}\mathbf{c} = \mathbf{0}, \tag{23}$$

due to the partition of unity of NURBS basis functions, where $\mathbf{c} \in \mathbf{R}^2$ is a constant vector. Thus, $\varepsilon_m^h = \gamma_s^h = \omega_b^h = 0$ for any $\mathbf{c}_T \in \mathbf{R}^2$, if the initial geometry is straight.

We only present the proof of vanishing shear strain if the initial geometry is circular or straight for the infinitesimal rigid body rotation of Eq. (5) and $\theta_{bI} = \theta_b^h = c_R$. Similar procedures can be straightforwardly applied to show the invariance of the membrane strain. First, for a circular geometry, substituting Eq. (5) into Eq. (16), and using the expression of $\tilde{\mathbf{I}}\mathbf{a}$ of Eq. (19) and the relation $\tilde{\mathbf{I}}^T = \tilde{\mathbf{I}}^{-1}$, we have the following:

$$\begin{aligned}\gamma_s^h &= c_R \sum_{I=1}^{n}\sum_{i=1}^{n}\left\{k W_I A_{Ii}^{-1}\mathbf{j}_1{}^T(\bar{\xi}_i) + W_{I,s}A_{Ii}^{-1}\mathbf{j}_2{}^T(\bar{\xi}_i)\right\}\tilde{\mathbf{I}}\left\{\mathbf{X}(\bar{\xi}_i) - \mathbf{X}_{ref}\right\} - c_R\sum_{i=1}^{n} W_I \\ &= -c_R \sum_{I=1}^{n}\sum_{i=1}^{n}\left\{W_I A_{Ii}^{-1}\mathbf{j}_1{}^T(\bar{\xi}_i) + W_{I,s}A_{Ii}^{-1}\mathbf{j}_2{}^T(\bar{\xi}_i)/k\right\}\tilde{\mathbf{I}}k\left\{\mathbf{X}_c - \mathbf{X}(\bar{\xi}_i)\right\} + \mathbf{a}^T(\mathbf{X}_c - \mathbf{X}_{ref}) - c_R. \end{aligned} \tag{24}$$

Then, using Eqs. (20) and (23), the shear strain of Eq. (24) can be shown to vanish, as follows:

$$\gamma_s^h = c_R \sum_{I=1}^{n}\sum_{i=1}^{n}\left\{W_I A_{Ii}^{-1}\mathbf{j}_1{}^T(\bar{\xi}_i) + W_{I,s}A_{Ii}^{-1}\mathbf{j}_2{}^T(\bar{\xi}_i)/k\right\}\mathbf{j}_1(\bar{\xi}_i) - c_R = c_R\sum_{I=1}^{n} W_I - c_R = 0. \tag{25}$$

Second, for straight geometry, $k = 0$ and $\mathbf{j}_2$ is a constant vector. Substituting Eq. (5) into (16), and using the relations $\mathbf{X}_{,s} = \sum_{I=1}^{n} W_{I,s}\mathbf{B}_I = \mathbf{j}_1$ and $\mathbf{j}_2 = \tilde{\mathbf{I}}\mathbf{j}_1$, we obtain the following:

$$\begin{aligned}\gamma_s^h &= c_R\mathbf{j}_2{}^T\tilde{\mathbf{I}}\sum_{I=1}^{n}\sum_{i=1}^{n} W_{I,s}A_{Ii}^{-1}\mathbf{X}(\bar{\xi}_i) - c_R\mathbf{j}_2{}^T\tilde{\mathbf{I}}\sum_{I=1}^{n} W_{I,s}\left(\sum_{i=1}^{n} A_{Ii}^{-1}\mathbf{X}_{ref}\right) - c_R \\ &= c_R\mathbf{j}_2{}^T\tilde{\mathbf{I}}\sum_{I=1}^{n} W_{I,s}\mathbf{B}_I - c_R\mathbf{j}_2{}^T\tilde{\mathbf{I}}\mathbf{X}_{ref}\sum_{I=1}^{n} W_{I,s} - c_R \\ &= c_R\mathbf{j}_2{}^T\mathbf{j}_2 - c_R = 0, \end{aligned} \tag{26}$$

for all $c_R \in \mathbf{R}$ and $\mathbf{X}_{ref} \in \mathbf{R}^2$. Therefore, the following observation is given.

Observation 2. The discretization of Eqs. (7) and (8) leads to the non-invariance of the approximated membrane strain of Eq. (9) and the shear strain of Eq. (10). However, in case the initial geometry is circular or straight, the strain measures remain invariant as well. Also, self-straining can be reduced through *h*-refinement as the initial curvature variation of elements decreases. The approximated bending strain is always invariant, regardless of the initial geometry.

Hereafter, the discretization using Eqs. (7) and (8) is denominated as "*Discretization* #1 (D#1)".

3. Locking-free invariant formulation

3.1. Invariant discretization using the global displacement field

We prove that the discretization of the global displacement vector instead of Eq. (7) can eliminate self-straining of the membrane and shear strain measures. The global displacement is discretized as

$$\hat{\mathbf{z}}^h = \sum_{I=1}^{n} W_I\hat{\mathbf{y}}_I, \tag{27}$$

where $\hat{\mathbf{y}}_I$ is the displacement coefficient corresponding to Ith control point. The approximated membrane and shear strain measures of Eq. (3) can be rewritten, using Eqs. (8) and (27), as

$$\left.\begin{aligned}\varepsilon_m^h &= \sum_{I=1}^{n}(W_{I,s}\hat{\mathbf{y}}_I)\cdot\mathbf{j}_1 \\ \gamma_s^h &= \sum_{I=1}^{n}\left\{(W_{I,s}\hat{\mathbf{y}}_I)\cdot\mathbf{j}_2 - W_I\theta_{bI}\right\}\end{aligned}\right\}. \tag{28}$$

To verify the invariance of the strain measures of Eq. (28), consider the rigid body translation expressed by $\hat{\mathbf{z}} = \mathbf{c}_T$ and the rotation angle $c_R = 0$. By the affine covariance property of NURBS basis function, $\hat{\mathbf{y}}_I = \mathbf{c}_T$ and $\theta_{bI} = c_R = 0$. Then, Eq. (28) is rewritten as

$$\left.\begin{aligned} \varepsilon_m^h &= (\mathbf{c}_T \cdot \mathbf{j}_1) \sum_{I=1}^{n} W_{I,s} = 0 \\ \gamma_s^h &= (\mathbf{c}_T \cdot \mathbf{j}_2) \sum_{I=1}^{n} W_{I,s} = 0 \end{aligned}\right\}, \tag{29}$$

for all $\mathbf{c}_T \in \mathbf{R}^2$ due to the partition of unity of NURBS basis function. Next, we consider the infinitesimal rigid body rotation expressed by a constant angle $c_R \in \mathbf{R}$. The affine covariance property of NURBS basis function enables to represent the rigid body rotation of physical domain as $\hat{\mathbf{y}}_I = c_R \tilde{\mathbf{I}}(\mathbf{B}_I - \mathbf{X}_{ref})$ and $\theta_{bI} = c_R$. Substituting into (28) gives

$$\begin{aligned} \varepsilon_m &= \sum_{I=1}^{n} \left\{ W_{I,s} c_R \tilde{\mathbf{I}}(\mathbf{B}_I - \mathbf{X}_{ref}) \right\} \cdot \mathbf{j}_1 \\ &= c_R \tilde{\mathbf{I}} \sum_{I=1}^{n} (W_{I,s} \mathbf{B}_I \cdot \mathbf{j}_1) - (c_R \tilde{\mathbf{I}} \mathbf{X}_{ref} \cdot \mathbf{j}_1) \sum_{I=1}^{n} W_{I,s} \\ &= c_R \tilde{\mathbf{I}} \mathbf{j}_1 \cdot \mathbf{j}_1 = 0 \end{aligned} \tag{30}$$

and

$$\begin{aligned} \gamma_s &= \sum_{I=1}^{n} \left\{ W_{I,s} c_R \tilde{\mathbf{I}}(\mathbf{B}_I - \mathbf{X}_{ref}) \right\} \cdot \mathbf{j}_2 - c_R \\ &= \sum_{I=1}^{n} W_{I,s} c_R \tilde{\mathbf{I}} \mathbf{B}_I \cdot \mathbf{j}_2 - (c_R \tilde{\mathbf{I}} \mathbf{X}_{ref} \cdot \mathbf{j}_2) \sum_{I=1}^{n} W_{I,s} - c_R \\ &= c_R \tilde{\mathbf{I}} \mathbf{j}_1 \cdot \mathbf{j}_2 - c_R = 0, \end{aligned} \tag{31}$$

for all $c_R \in \mathbf{R}$, where $\mathbf{X}_{,s} = \sum_{I=1}^{n} W_{I,s} \mathbf{B}_I = \mathbf{j}_1$ and $\mathbf{j}_2 = \tilde{\mathbf{I}} \mathbf{j}_1$ are used.

Observation 3. The approximated membrane and shear strain measures in Eq. (28) are invariant regardless of the initial geometry.

Hereafter, the discretization using Eqs. (8) and (27) is denominated as "*Discretization* #2 (D#2)".

3.2. Locking-free invariant formulation

The proposed invariant formulation (D#2) is combined with the $\bar{B}$ projection method for NURBS basis functions whereas the formulation D#1 is used in Bouclier et al. [1]. Basically, in the $\bar{B}$ projection method, the approximated strain field described in the space Q_p of pth order NURBS basis functions is linearly projected onto the space Q_{p-1} of $(p-1)$th order. The detailed description of selecting the number of basis functions and the set of knots in the space Q_{p-1} can be found in Bouclier et al. [1]. The strain field in the space Q_p is projected onto the space Q_{p-1} as

$$\left.\begin{aligned} \tilde{\varepsilon}_m^h &= \sum_{I=1}^{\tilde{n}} \tilde{W}_I \tilde{\varepsilon}_{mI}^h \\ \tilde{\gamma}_s^h &= \sum_{I=1}^{\tilde{n}} \tilde{W}_I \tilde{\gamma}_{sI}^h \end{aligned}\right\}, \tag{32}$$

where $\tilde{n}$ denotes the number of basis functions in the lower order space. $\tilde{W}_I$ is the corresponding lower order basis function. Then, the equivalence between the original and the projected strain fields is weakly expressed, for all

$v \in Q_{p-1}$, as

$$\left.\begin{aligned} \int_\Omega v\varepsilon_m^h d\Omega &= \int_\Omega v \sum_{I=1}^{\tilde{n}} \tilde{W}_I \tilde{\varepsilon}_{mI}^h d\Omega \\ \int_\Omega v\gamma_s^h d\Omega &= \int_\Omega v \sum_{I=1}^{\tilde{n}} \tilde{W}_I \tilde{\gamma}_{sI}^h d\Omega \end{aligned}\right\}. \tag{33}$$

The test function $v \in Q_{p-1}$ can be expressed by the lower order basis functions $\tilde{W}_I$ so that

$$\left.\begin{aligned} \int_\Omega \varepsilon_m^h \sum_{K=1}^{\tilde{n}} \tilde{W}_K v_K d\Omega &= \int_\Omega \sum_{I,J=1}^{\tilde{n}} \tilde{W}_I \tilde{W}_J \tilde{\varepsilon}_{mI}^h v_J d\Omega \\ \int_\Omega \gamma_s^h \sum_{K=1}^{\tilde{n}} \tilde{W}_K v_K d\Omega &= \int_\Omega \sum_{I,J=1}^{\tilde{n}} \tilde{W}_I \tilde{W}_J \tilde{\gamma}_{sI}^h v_J d\Omega \end{aligned}\right\}. \tag{34}$$

Then, defining $\tilde{M}_{IJ} = \int_\Omega \tilde{W}_I \tilde{W}_J d\Omega$, the coefficients of the projected strain field are obtained as

$$\left.\begin{aligned} \tilde{\varepsilon}_{mI}^h &= \sum_{J=1}^{\tilde{n}} \tilde{M}_{IJ}^{-1} \int_\Omega \tilde{W}_J \varepsilon_m^h d\Omega \\ \tilde{\gamma}_{sI}^h &= \sum_{J=1}^{\tilde{n}} \tilde{M}_{IJ}^{-1} \int_\Omega \tilde{W}_J \gamma_s^h d\Omega \end{aligned}\right\}. \tag{35}$$

In the proposed invariant formulation (D#2) using Eqs. (28) and (32), $\tilde{\varepsilon}_m^h$ and $\tilde{\gamma}_s^h$ are derived as

$$\left.\begin{aligned} \tilde{\varepsilon}_m^h &= \sum_{I,J=1}^{\tilde{n}} \sum_{K=1}^{n} \tilde{W}_I \tilde{M}_{IJ}^{-1} \int_\Omega \tilde{W}_J (W_{K,s} \hat{\mathbf{y}}_K) \cdot \mathbf{j}_1 d\Omega \\ \tilde{\gamma}_s^h &= \sum_{I,J=1}^{\tilde{n}} \sum_{K=1}^{n} \tilde{W}_I \tilde{M}_{IJ}^{-1} \int_\Omega \tilde{W}_J \left\{ (W_{K,s} \hat{\mathbf{y}}_K) \cdot \mathbf{j}_2 - W_K \theta_{bK} \right\} d\Omega \end{aligned}\right\}. \tag{36}$$

Also, by the formulation D#1, as in Ref. [1], they can be derived as

$$\left.\begin{aligned} \tilde{\varepsilon}_m^h &= \sum_{I,J=1}^{\tilde{n}} \sum_{K=1}^{n} \tilde{W}_I \tilde{M}_{IJ}^{-1} \int_\Omega \tilde{W}_J (W_{K,s} y_{1K} - k W_K y_{2K}) d\Omega \\ \tilde{\gamma}_s^h &= \sum_{I,J=1}^{\tilde{n}} \sum_{K=1}^{n} \tilde{W}_I \tilde{M}_{IJ}^{-1} \int_\Omega \tilde{W}_J (k W_K y_{1K} + W_{K,s} y_{2K} - W_K \theta_{bK}) d\Omega \end{aligned}\right\}. \tag{37}$$

4. Numerical examples

4.1. Self-straining in curved beam models

We consider two curved beam models; model #1 and model #2. The geometry of model #1 is described by cubic B-spline basis functions and four control points, as shown in Fig. 1(a). The vertical coordinates (H) of control points B and C are altered to investigate the dependence of non-invariance on the initial geometry. Fig. 1(b) shows the norm of vector $\mathbf{a}$ in Eq. (18) for two cases; $H = 0.125$ and $H = 1$ over the half of the parametric domain ($0 \leq \xi < 0.5$) due to the symmetry of the curve about the mid-point ($\xi = 0.5$), where $\mathbf{a} = \mathbf{0}$ due to the point symmetry. It shows that $\mathbf{a}$ does not vanish in the domain. In other words, the membrane and shear strains are generated during rigid body motions. Fig. 1(c) shows that the L_2 norm of $\mathbf{a}$ increases as we increase H, which indicates that self-straining gets worse as the initial curvature variation of domain increases.

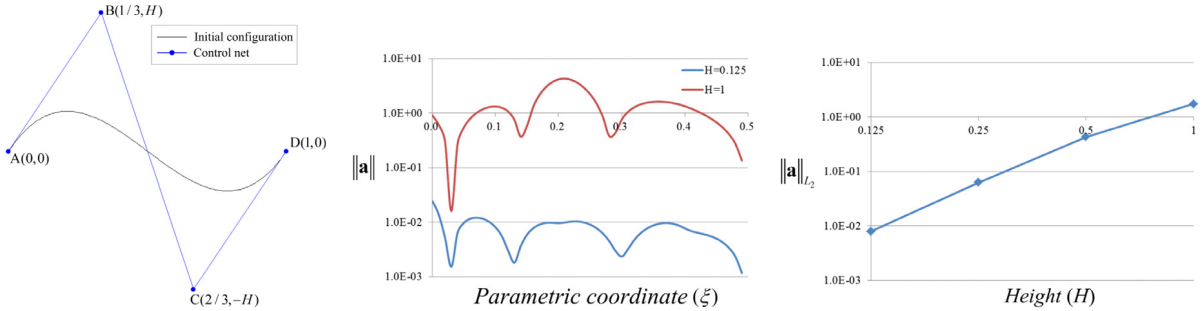

(a) Model description. (b) Distribution of $\|\mathbf{a}\|$. (c) $\|\mathbf{a}\|_{L_2}$ for increasing H.

Fig. 1. Non-invariance of model #1.

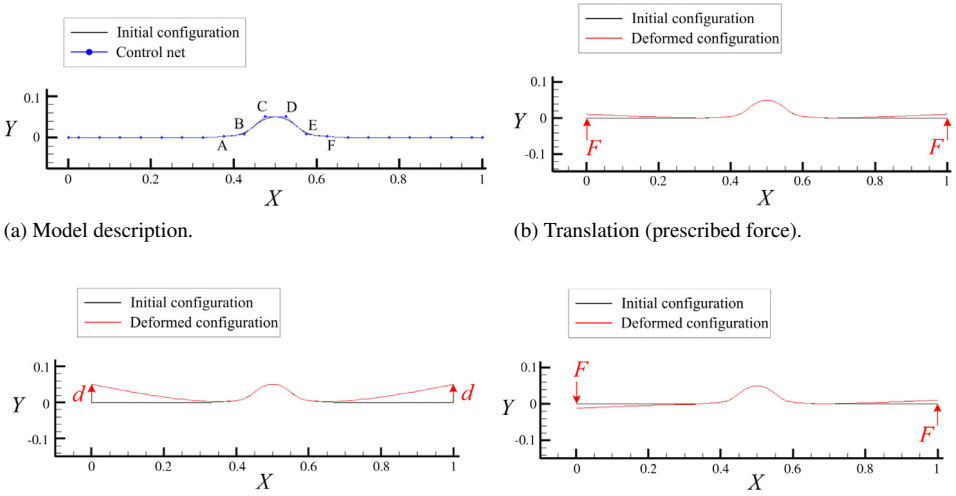

(a) Model description. (b) Translation (prescribed force).

(c) Translation (prescribed displacement). (d) Rotation.

Fig. 2. Inability of model #2 to represent rigid body motions due to self-straining.

Model #2 is constructed as a straight geometry with quadratic B-spline basis functions and uniform knot distribution. Then, 6 control points in the middle of the beam are vertically moved to the positions A(0.0025), B(0.0075), C(0.05), D(0.05), E(0.0075), and F(0.0025), where the numbers in the parentheses represent Y-coordinates as shown in Fig. 2(a).

To verify self-straining of model #2 using the formulation D#1, three loading conditions (concentrated force $F = 100$, displacement $d = 0.05$) are imposed for rigid body translation (Fig. 2(b) and (c)) and the infinitesimal rigid body rotation (Fig. 2(d)). Three Gauss integration points (full integration) are used for each element. Even though no essential boundary conditions are imposed, spurious constraints restrict rigid body motions due to self-straining in the middle region of large curvature. For the same problems, the formulation D#2 results in singular stiffness matrices properly. In the following section, it is shown that these self-straining phenomena have significant influence on the accuracy of response analysis.

4.2. *Errors in displacement field due to self-straining*

For both of the models #1 and #2, pure bending problems are considered with a clamped boundary condition and a sinusoidal loading of distributed moment as follows:

$$m(s) = EI\left(\frac{\pi}{2L}\right)^2 \sin\left(\frac{\pi}{2L}s\right), \tag{38}$$

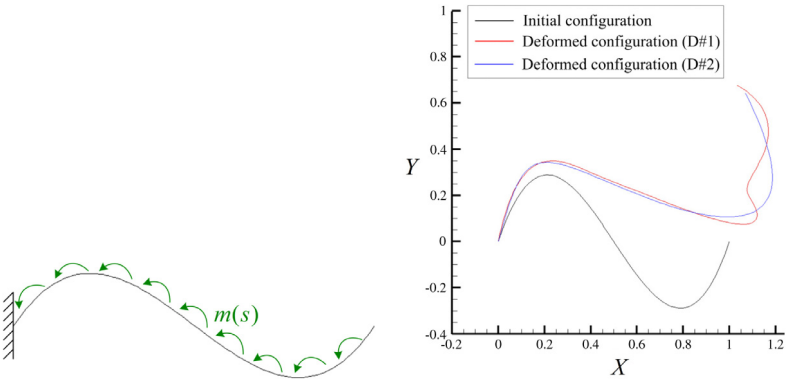

(a) Problem description. (b) Deformation (SRI).

Fig. 3. Response analysis of model #1 ($H = 1$).

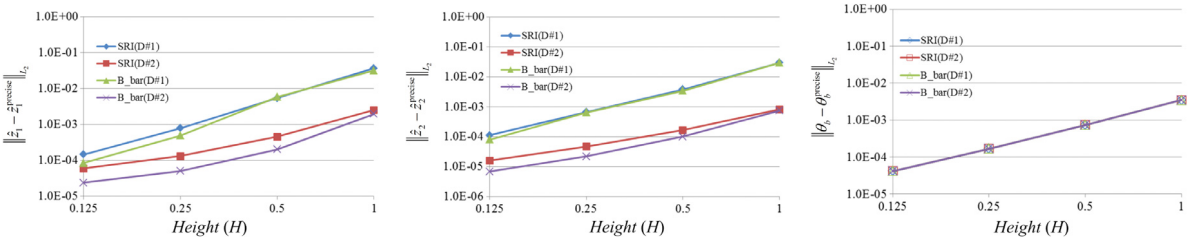

(a) X-directional displacement. (b) Y-directional displacement. (c) Rotation.

Fig. 4. Dependence on vertical coordinate H.

where s and L are the arc-length coordinate and the length of the beam, respectively. $E = 210$ GPa and $I = bh^3/12$ are the Young's modulus and the second moment of inertia, respectively. $b = 0.01$ and h are respectively the width and thickness of beam, and Poisson's ratio is set to be zero. In this paper, two locking-free formulations are considered; the selective reduced integration (SRI) [2] and the $\bar{B}$ projection method [1]. Also, the effect of replacing the strain field discretization with D#2 is investigated. The exact solution of rotation angle for this problem is derived in Adam et al. [2] as Eq. (A.1), which involves the arc-length coordinate s. We further extend the exact solution to the exact solution of the first order derivatives of global displacements, which is followed by retrieving the global displacement field through numerical integration of Eq. (A.5). As the arc-length coordinate s is also calculated by the numerical integration, the obtained reference solutions for both of displacement and rotation are not exact. However, we calculate these numerical integrations using enough number of elements and Gauss integration points, so that the solutions are denominated as precise solutions. Detailed expressions for the reference solutions can be found in the Appendix.

Consider the model #1 of cantilever with the vertical coordinate $H = 1$ and thickness $h = 0.01$ as shown in Fig. 3(a). Fig. 3(b) illustrates the deformed configurations of the 5 elements cantilever beam under two different formulations D#1 and D#2, combined with the SRI.

The result of formulation D#1 is significantly deteriorated, compared with that of formulation D#2. Fig. 4 shows the dependence of L_2 error of responses on the vertical coordinate H. As increasing the H, the error of displacement obtained by the formulation D#1 significantly increases, which is mainly due to the numerical instability caused by self-straining. It is noted that, since the approximated bending strain measure is invariant, the rotation angle is not affected by self-straining and shows good agreement with the precise solution even if the formulation D#1 is used.

Fig. 5(a) shows that the L_2 norm of vector $\mathbf{a}$ reduces according to h-refinement, as mentioned in Observation 2. The spurious strain energy generated in the rigid body motions reduces as the mesh is refined. However, the non-invariance still persists and consequently yields overall poor accuracy of the displacement field. Fig. 5(b) and (c) present the convergence of displacements. The invariant formulation D#2 gives much more accurate results than D#1 for both SRI and $\bar{B}$ projection method.

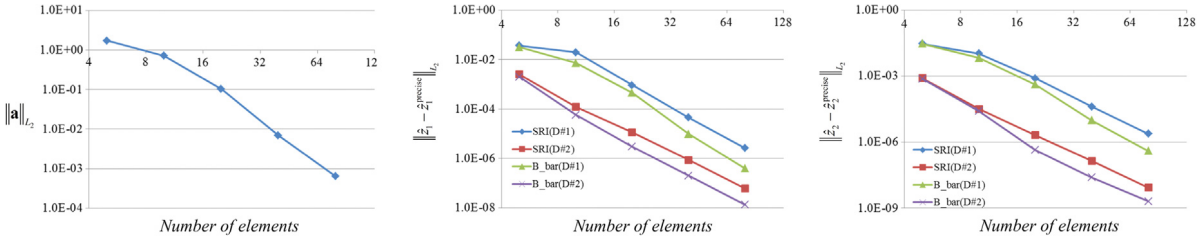

(a) Self-straining. (b) X-directional displacement. (c) Y-directional displacement.

Fig. 5. Displacement comparison in discretization methods (D#1 and D#2).

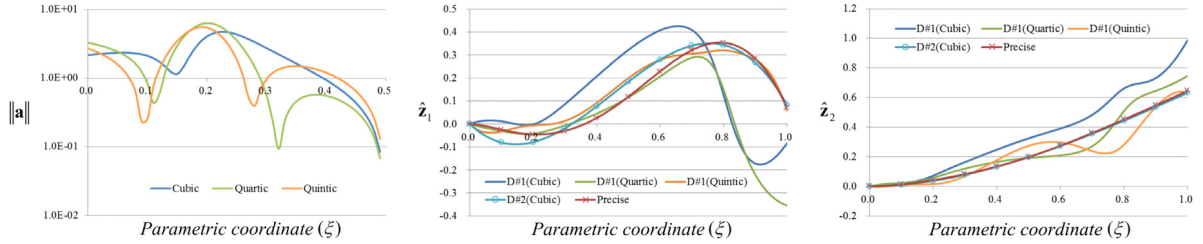

(a) Self-straining. (b) X-directional displacement. (c) Y-directional displacement.

Fig. 6. Comparison of displacement fields (For interpretation of the references to color in this figure legend, the reader is referred to the web version of this article.)

To investigate the effect of higher-order discretization on self-straining, we consider the single element cantilever of model #1 with the vertical coordinate $H = 1$ and thickness $h = 0.01$ as shown in Fig. 3(a). For three different orders of basis function, Fig. 6(a) shows the norm of the vector $\mathbf{a}$ in Eq. (18) over the half of the parametric domain ($0 \leq \xi < 0.5$) due to the point symmetry of the curve about the mid-point ($\xi = 0.5$) where $\mathbf{a} = \mathbf{0}$. As shown in Fig. 6(a), the self-straining is still persisting in the higher order discretization, which implies that the p-refinement does not effectively reduce the numerical instability. Consequently, compared with the results of D#2 using cubic basis function (Light blue) in Fig. 6(b) and (c), the displacement field obtained by D#1 is significantly deteriorated with oscillations, even employing quartic (Green) and quintic (Orange) basis functions.

Consider the model #2 of cantilever model with the number of elements NE and thickness $h = 0.01$, as shown in Fig. 7(a). Fig. 7(b) and (c) illustrate the deformed configurations obtained by the formulations D#1 and D#2, combined with the SRI. The displacement field obtained by the D#1 undergoes severe oscillations from the position where the abrupt change of curvature occurs, as shown in Fig. 7(b). As the mesh is refined, the amplitude of oscillations is significantly reduced. This can be explained by the reduction of self-straining due to the h-refinement (Observation 2). However, compared with the results of D#2 using coarse mesh shown in Fig. 7(c), it is apparent that the persisting oscillations in the refined model significantly deteriorate the quality of responses.

Fig. 8 shows the global displacement fields using the SRI combined with the formulations D#1 and D#2. The displacement fields using the D#1 exhibit serious oscillations persisting even in the refined model, even though the overall accuracy is improved. The rotation angle is always accurate regardless of discretization method, due to the invariance of the approximated bending strain measure.

Fig. 9 shows the comparison of strain fields, where the vertical dotted lines represent the element boundaries. We notice that several discontinuities appear in the strain fields using the D#1, due to the discontinuity of initial curvature. In both formulations of D#1 and D#2, the vanishing points of membrane and shear strains coincide with the position of integration points in the SRI [2]. However, it is obvious that the amplitude of strains in the D#1 is much larger than that of the D#2. This is mainly due to the numerical instability triggered by self-straining around the region of large curvature and its propagation due to the higher order continuity of displacement field. The bending strain is accurate, regardless of discretization method, due to its invariance property.

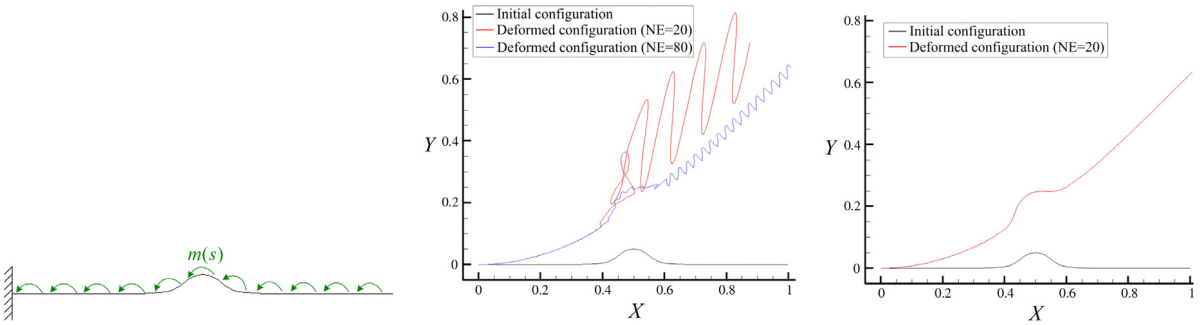

(a) Problem description. (b) Deformation (SRI, D#1). (c) Deformation (SRI, D#2).

Fig. 7. Comparison of configuration (For interpretation of the references to color in this figure legend, the reader is referred to the web version of this article.)

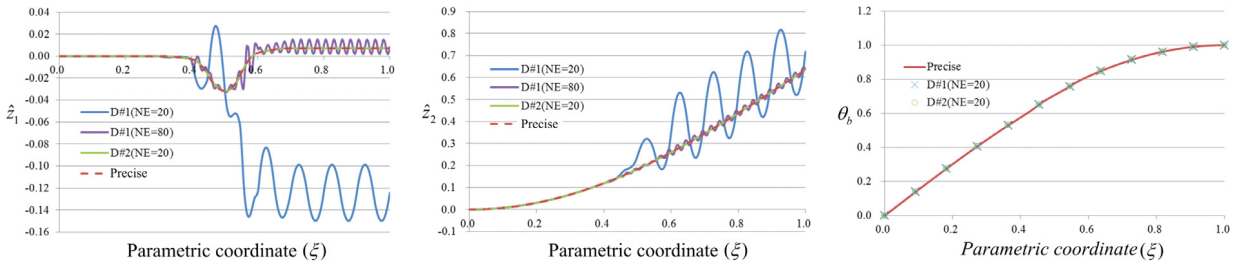

(a) X-direction. (b) Y-direction. (c) Rotation.

Fig. 8. Comparison of displacement and rotation fields (For interpretation of the references to color in this figure legend, the reader is referred to the web version of this article.)

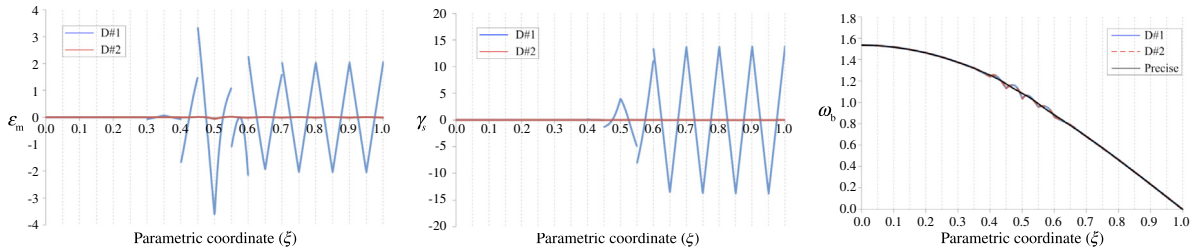

(a) Membrane. (b) Shear. (c) Bending.

Fig. 9. Comparison of strain fields.

4.3. Comparison of the conventional and invariant locking-free formulations

We compare the accuracy of results obtained from the conventional (D#1) and invariant (D#2) locking-free formulations (SRI and $\bar{B}$ projection method). Consider again the model #2 whose initial length is $L = 1.02$, with the distributed moment loading and clamped boundary condition, as described in Fig. 7(a). 20 elements with uniform knot distribution are used. Fig. 10 shows the change of the relative L_2 error of responses as we increase the slenderness ratio (L/h). If the full integration (3 integration points for each element) is used in the formulation D#1, the deformation (Green) vanishes even for small slenderness ratio. This is due to self-straining of the membrane and shear strains which absorb the major part of the strain energy, especially in the region of large curvature. If the invariant formulation D#2 is employed, the accuracy of responses (Orange) in small slenderness ratio is significantly improved but deteriorated due to membrane and shear locking troubles as the slenderness ratio increases. To alleviate these locking troubles, the SRI [2] and the $\bar{B}$ projection method [1] are employed.

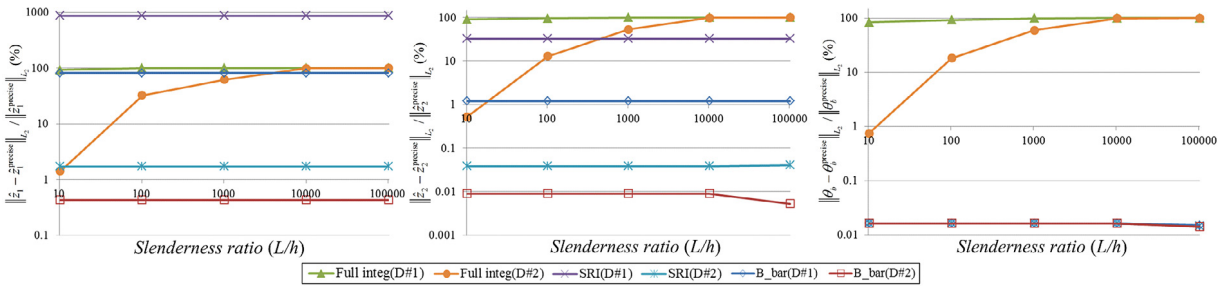

(a) X-displacement. (b) Y-displacement. (c) Rotation.

Fig. 10. Comparison of relative L_2 errors in model #2 (For interpretation of the references to color in this figure legend, the reader is referred to the web version of this article.)

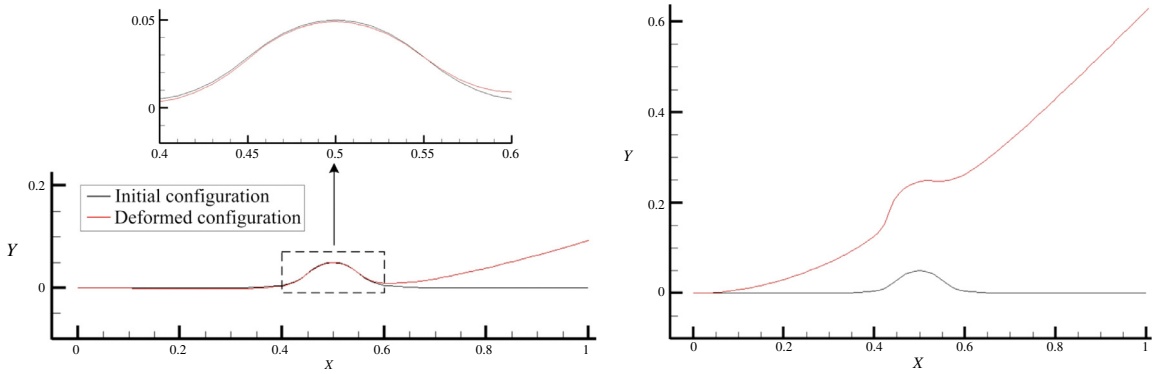

(a) Formulation D#1. (b) Invariant formulation D#2.

Fig. 11. Comparison of deformed configurations.

Table 1
Comparison of contribution in total strain energy.

	Formulation D#1				Invariant formulation D#2			
	E_{total}	$E_{membrane}$	E_{shear}	$E_{bending}$	E_{total}	$E_{membrane}$	E_{shear}	$E_{bending}$
	1.93E+04	2.83E+03	7.17E+03	9.29E+03	4.48E+04	1.03E+03	4.59E+02	4.33E+04
Ratio (%)	100	14.65	37.17	48.17	100	2.31	1.03	96.67

As shown in Fig. 10, although locking-free formulations combined with D#1 eliminate the dependence of solution on the slenderness ratio, the accuracy (Purple, Blue) is still not satisfactory. This inaccuracy stems from the severe numerical instability triggered by self-straining, as illustrated in Figs. 7 and 8. As the invariant formulation D#2 is employed, the self-straining problem is resolved and the accuracy of responses is significantly improved in all the slenderness ratios (Light blue, Red).

Fig. 11 illustrates the deformed configurations obtained from D#1 and D#2 using the full integration, for the case of slenderness ratio $L/h = 10.2$. As shown in the curved region of Fig. 11(a), the beam seems to be constrained by the spurious constraint that restricts the deformation of beam to be very small.

Table 1 presents the strain energy of each deformation mode and its ratio to the total strain energy in the curved region ($0.4 \leq X \leq 0.6$). In the result of D#1, the membrane and shear strain energy constitutes a half of total strain energy, which is mainly due to the spurious membrane and shear strains generated by self-straining that appears as a serious spurious constraint in the curved region. This trouble is fully resolved through the invariant formulation D#2, as shown in Fig. 11(b). Table 1 shows that the beam model nearly recovers the pure bending nature.

5. Conclusions

In this paper, we observe self-straining phenomena in existing isogeometric formulations of curved Timoshenko beams. Self-straining gets worse as the curvature variation of domain increases and has significant influence on the accuracy of response analysis. Self-straining can be reduced more or less through h-refinement as the initial curvature variation of elements decreases, however, it is apparent that the persisting oscillations in the refined model significantly deteriorate the response quality. In the existing formulation, a numerical example demonstrates that the membrane and shear strain energy constitutes a half of total strain energy, which is mainly due to the spurious membrane and shear strains generated by self-straining that appears as a serious spurious constraint in the curved region. In the proposed invariant formulation that uses the discretization of the global displacement field, it is shown that self-straining can be completely eliminated. Through various numerical examples, we verify the significance of the proposed invariant formulation to achieve accurate results for arbitrarily curved beams.

Acknowledgment

This work was supported by the National Research Foundation of Korea (NRF) grant funded by the Korea government (MSIP) (No. 2010-0018282).

Appendix

For the sinusoidal moment loading condition of Eq. (38), Adam et al. [2] derived the exact solution of the rotation angle as

$$\theta_b(s) = \sin\left(\frac{\pi}{2L}s\right). \tag{A.1}$$

Since the membrane and shear strains vanish due to the pure bending nature, using Eq. (3), for a given θ_b and $\forall s \in [0, L]$, we have two differential equations for the global displacement vector $\hat{\mathbf{z}}$ as

$$\left.\begin{aligned} \hat{\mathbf{z}}_{,s} \cdot \mathbf{j}_1 &= 0 \\ \hat{\mathbf{z}}_{,s} \cdot \mathbf{j}_2 &= \theta_b \end{aligned}\right\}. \tag{A.2}$$

Eq. (A.2) can be rewritten as

$$\begin{bmatrix} (\mathbf{j}_1)_1 & (\mathbf{j}_1)_2 \\ (\mathbf{j}_2)_1 & (\mathbf{j}_2)_2 \end{bmatrix} \hat{\mathbf{z}}_{,s} = \begin{Bmatrix} 0 \\ \theta_b \end{Bmatrix}, \ \forall s \in [0, L]. \tag{A.3}$$

Therefore, the exact solution of $\hat{\mathbf{z}}_{,s}$ is obtained as

$$\hat{\mathbf{z}}_{,s} = \frac{1}{(\mathbf{j}_1)_1(\mathbf{j}_2)_2 - (\mathbf{j}_1)_2(\mathbf{j}_2)_1} \begin{bmatrix} (\mathbf{j}_2)_2 & -(\mathbf{j}_1)_2 \\ -(\mathbf{j}_2)_1 & (\mathbf{j}_1)_1 \end{bmatrix} \begin{Bmatrix} 0 \\ \theta_b \end{Bmatrix} = \begin{Bmatrix} -(\mathbf{j}_1)_2 \\ (\mathbf{j}_1)_1 \end{Bmatrix} \theta_b, \tag{A.4}$$

since $(\mathbf{j}_1)_1(\mathbf{j}_2)_2 - (\mathbf{j}_1)_2(\mathbf{j}_2)_1 = \|\mathbf{j}_1 \times \mathbf{j}_2\| = 1$. Considering the clamped boundary condition, we have the final expression of the global displacement field as

$$\hat{\mathbf{z}}(s) = \int_0^s \begin{Bmatrix} -(\mathbf{j}_1)_2(\tilde{s}) \\ (\mathbf{j}_1)_1(\tilde{s}) \end{Bmatrix} \theta_b(\tilde{s}) d\tilde{s}. \tag{A.5}$$

References

[1] R. Bouclier, T. Elguedj, A. Combescure, Locking free isogeometric formulations of curved thick beams, Comput. Methods Appl. Mech. Engrg. 245 (2012) 144–162.
[2] C. Adam, S. Bouabdallah, M. Zarroug, H. Maitournam, Improved numerical integration for locking treatment in isogeometric structural elements, part i: Beams, Comput. Methods Appl. Mech. Engrg. 279 (2014) 1–28.
[3] F. Armero, J. Valverde, Invariant hermitian finite elements for thin kirchhoff rods. i: The linear plane case, Comput. Methods Appl. Mech. Engrg. 213 (2012) 427–457.
[4] L. Piegl, W. Tiller, The NURBS Book, Springer Science & Business Media, 2012.